2018 IEEE/RSJ International Conference on Intelligent Robots and Systems (IROS)
Madrid, Spain, October 1-5, 2018

Design of a Lightweight, Ergonomic Manipulator for Enabling Expressive Gesturing in Telepresence Robots

James T. Slack[1], Kyle DeProw[1], Zachary Anderson[2], Ricardo M. Albacete Di Bartolomeo[1], Jerry B. Weinberg[2] (IEEE Member), Jenna L. Gorlewicz[1] (IEEE Member)

Abstract— **Recent research on telepresence robots demonstrates that while they enable new heights of remote communication, there still exists challenges for both local and remote users in creating a connectedness one only encounters in face-to-face interactions. A large part of communication is beyond hearing and vision. Tangible interactions, expressive gestures, and physical referencing represent three of the primary social behaviors missing in the current telepresence experience. There is an inherent, subconscious quality to these physical actions that has been shown to allow more expressive and engaging communication. In this project we present the design, fabrication, and initial performance validation of a lightweight, ergonomic manipulator with a heavy, anthropomorphic end effector that enables gesturing capabilities for telepresence interactions.**

I. INTRODUCTION

Commercial telepresence robots (e.g. Anybots QB, VGo, Beam, Double Telepresence Robot) are gaining traction in numerous applications including business, education, healthcare, and social interaction for the elderly (e.g. [1][2] [3][4][5][6][7]). Telepresence robots enable video conferencing on a mobile, robotic platform, situating themselves between basic video conferencing and complex human-like robots. While such platforms allow the remote user to be more "present," the lack of tangible interactions and expressive gesturing capabilities can leave the user feeling helpless, and leave colleagues confused with how to interact with the robot. These qualitative notions are backed by research on social telepresence, which have shown that a human-like teleoperated robot enhances social connectedness compared to audio/video conferencing [8]. Prior research has also suggested that adding a tangible hand to a teleconferencing screen or having humanoid limbs on a robot may increase local users' abilities to connect with and engage with the remote user on a nonverbal level [9][10][11].

In this paper, we present the design, fabrication, and performance validation of a lightweight manipulator designed specifically for attachment to a telepresence robot. Our manipulator embodies human-like functionality, enabling the three primary social behaviors of tangible interactions, expressive gestures, and referencing by pointing [11], while also being lightweight and of a small-form factor for carrying onboard the telepresence platform. This work lays the foundation for the larger vision of this project, which is to expand the social experience between the local and remote users by evolving the remote user interface with a hands-free, one-to-one mapping of their gestures to the robot manipulator's movements and enhance the local user's experience with the added communication channel of the remote user's gestures expressed through the robot manipulator.

[1]Department of Mechanical and Aerospace Engineering, Saint Louis University, Saint Louis, MO 63103, USA
[2]Department of Computer Science, Southern Illinois University of Edwardsville, IL 62025, USA

II. TELEPRESENCE ROBOT PLATFORM

In this work, we are leveraging a commercially available telepresence robot - the Anybots, Inc. QB 2.0 (Figure 5 (Left)). We chose the QB platform because of its unique set of customizable hardware and accessible software tools, which is not common among other commercial platforms. The hardware of QB has several advantages. Large wheels enable it to drive over raised surfaces up to 2"; its small footprint takes up only as much space as a person; and it has a payload capacity of 20kg while still maintaining gyroscopic stability. The software of QB also enables users to access and control QB from anywhere through a web browser, and a developer's kit is available to customize the software. This customization and accessibility is necessary for seamless integration and operation of our manipulator.

III. MANIPULATOR DESIGN

A. Background

In this project we focus on manipulators designed to look and function similar to human arms and hands as these provide the largest enhancement to video-mediated interactions [11]. Several humanoid robots exist with two arms and 5-fingered hands which look and interact like humans. Examples include ARMAR-3 [12], Honda's Asimo [13], Robonaut [14], and iCub [15], to name a few. Though these arms do claim anthropomorphism through first degree approximation [12], they are unsuitable in scale or weight for our needs.

There also exist several hand designs meant to replicate the anatomy of the human hand. Examples include TUAT, a 20 DOF hand designed for use on the ARMAR robot [16], and the Robonaut hand, which is highly anthropomorphic and is close in strength and kinematics to that of an astronaut's hand in a space suit [14]. The RCH-1 hand is also 5 fingered with 6 DOFs and has embedded tactile sensors for force sensing [17]. In an effort to trade-off realism for simpler designs, researchers have generated several three finger (e.g. the JACO arm and HRP3 [18]) and four finger (e.g. [19], [20]) hand designs while exploring alternative actuation methods such as fluid power [21], pneumatic artificial muscles [22], and

978-1-5386-8094-0/18/$31.00 ©2018 IEEE

wire/tendon actuation [23], [17]. The challenge with many of the above hand designs is their lacking anthropomorphism both for enhancing the visual connection to the remote user and for the haptic feedback a realistic hand provides[11].

In this work, we build upon these prior efforts, designing a manipulator that trades off complexity for realism and portability, is able to support a heavy, realistic hand, and is suited for integration on telepresence platforms.

B. Design Constraints

The design constraints are dictated by the QB platform itself, the expressive behaviors we wish to replicate, and the aesthetics of the arm. The constraints from QB are that the arm and all electronic components must not exceed its 20kg payload capacity; all actuation must be able to run from a power source of 14.8 Volts and be able to be carried onboard QB (no tether); it must be designed in proportion with QB's size; it must anchor around QB's neck; and it must not alter QB's stability. The behaviors we wish to replicate are centered on the primary social behaviors: (1) tangible interactions, (2) expressive gestures, and (3) referencing by pointing [24]. From an aesthetic perspective, the manipulator must impart anthropomorphism but also be fluent with the rest of QB's persona, so as to not appear "too human-like" for the platform itself.

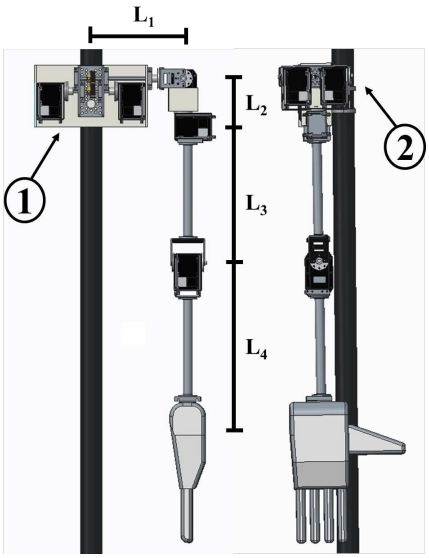

Fig. 1. The design of our manipulator created in Creo Parametric 4.0. (Left) Rear view (thumb facing into page) and (Right) Right side view. L_1, L_2, L_3, L_4 are the link lengths chosen based on anthropomorphic data of a *1.65m* tall person. The subsystem of the shoulder joint responsible for internal/external rotation is represented as Group 1, labeled as ①. The subsystem responsible for transverse abduction is represented as Group 2, labeled as ②.

C. Hand and Arm Design

From the above criteria, two key design objectives emerged: (1) a 5-fingered hand design and (2) a 4 DOF modular arm design.

Our design, shown in Figure 1, was created in Creo Parametric 4.0. The 5-fingered hand design was chosen as it is necessary to replicate fine motor behaviors (particularly pointing and realistic hand-shaking [11]) and to embody anthropomorphism. We chose the Open Bionics Ada Hand, shown in Figure 2, for its realism, dexterity, and simple, compact actuation (5 linear actuators in the palm). It is 3D printed Ninjaflex material, is comparable in size to a human hand, and weighs $330g$, making the hand 29 percent of the overall weight past the shoulder.

For the arm, the compromise of complexity with human-like motion guided our decisions. We evaluated both 4 DOF and 5 DOF design ideas. We ultimately chose a 4 DOF design because the payoff for reducing additional weight, torque, and power requirements was worth more from an implementation perspective than the functionality gained with adding a 5th DOF for wrist rotation. Additionally, we determined that the 4 DOF design has enough capacity to mimic the gross motor movements we wish to achieve, and that manipulation of the medial joint provided enough flexibility to achieve wrist/hand configurations desired in the expressive gestures listed. This is illustrated in Figure 2, where the manipulator is in a handshake configuration comparable to a human handshake with exaggerated tilt. The 4 DOF design consists of a 3 DOF shoulder joint and 1 DOF elbow joint, as seen in Figure 1. A 3 DOF shoulder joint in combination with a 1 DOF elbow is desirable over a 2 DOF shoulder joint and 2 DOF elbow because of the decreased overall system moment without sacrificing functionality. The joint responsible for internal/external rotation is centered on the midline of QB to mitigate unintended moments. Rigid links connect the shoulder to elbow and elbow to wrist. The lengths of the shoulder girdle, upper arm, and forearm segments are based on anthropomorphic data for a human $1.65m$ tall [25], the operating height of QB. The distance laterally from the midline of the body to the midpoint of the shoulder joint is $170.0mm$, represented as L_1 in Figure 1. The length from the shoulder to the elbow (upper arm) is $265.0mm$ $(L_2 + L_3)$. The length from the elbow to the wrist is $269.0mm$ (L_4). The hand is directly coupled to the forearm.

A consequence of a high-functioning hand on a lightweight manipulator is the large increase in required torque and power consumption. The largest static torque

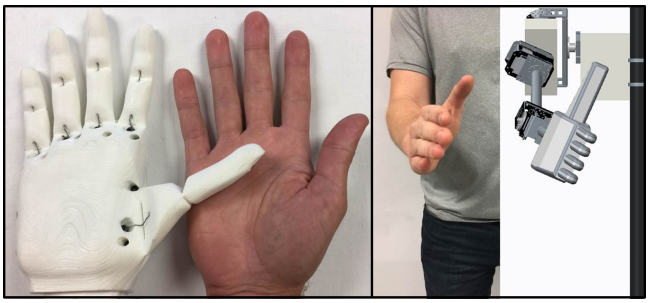

Fig. 2. Left: The hand, an Open Bionics Ada Hand, used in the manipulator design compared with a human hand. Right: The 4 DOF manipulator replicating normal handshake tilt.

the manipulator will have to support is when the arm is held horizontally outward (parallel to the ground). In this instance, the subsystem of the shoulder joint responsible for internal/external rotation, illustrated as Group 1 in Figure 1, will need to supply a calculated maximum torque of $2.92Nm$. The largest speed requirement the manipulator will see occurs during a one-quarter rotation for shoulder adduction. At maximum torque, this corresponds to a 90° rotation of the motors associated with the shoulder joint (Groups 1 and 2 in Figure 1) in $0.6s$. This speed is within normal non-duress human speed [26] and reflects a reasonable speed ceiling for operation. The prototype of the design is presented in Section V.

IV. Modeling and Simulation

This section presents forward and inverse kinematic modeling with workspace simulation.

A. Forward Kinematics

1) Denavit-Hartenberg Parameters: By assigning frames to the manipulator in Figure 3 and computing the Denavit-Hartenberg parameters, we can obtain a homogeneous transformation matrix for our manipulator, which represents its forward kinematics. The representation of our manipulator used for the D-H parameterization is shown in Figure 3 and Table I.

TABLE I
THE DENAVIT-HARTENBURG PARAMETERS OF OUR MANIPULATOR.

n	θ_n ($^\circ$)	α_n ($^\circ$)	d_n (mm)	r_n (mm)
1	0	0	0	0
2	θ_1^*	-90	L_1	0
3	θ_2^*	90	0	0
4	θ_3^*	-90	$L_2 + L_3$	0
5	θ_4^*	0	0	L_4

The revolute angles (θ_1^*, θ_2^*, θ_3^*, θ_4^*) are variables corresponding to human arm movements interpreted from the remote user via a Xbox Kinect (discussed more in Section IV-B) corresponding to frames (n) mapped from physical joints on the manipulator. The angle α_n is the angle of rotation about the x-axis of frame $n-1$ to n. The link lengths in columns d_n (distance in z-axis from $n-1$) and r_n (distance in x-axis from $n-1$) are determined from Section III and shown in Figure 3. The five transformation matrices responsible for determining the relationship between the base frame and the end effector can be found with:

$$T_{n-1}^{n} = \begin{bmatrix} C\theta_n & -S\theta_n C\alpha_n & S\theta_n S\alpha_n & r_n C\theta_n \\ S\theta_n & C\theta_n C\alpha_n & -C\theta_n S\alpha_n & r_n S\theta_n \\ 0 & S\alpha_n & C\alpha_n & d_n \\ 0 & 0 & 0 & 1 \end{bmatrix} \quad (1)$$

where S and C correspond to *sine* and *cosine* respectively.

The resulting transformation matrix from the middle of QB's shoulders (Frame 1) to the palm of the hand (Frame 5) is given as:

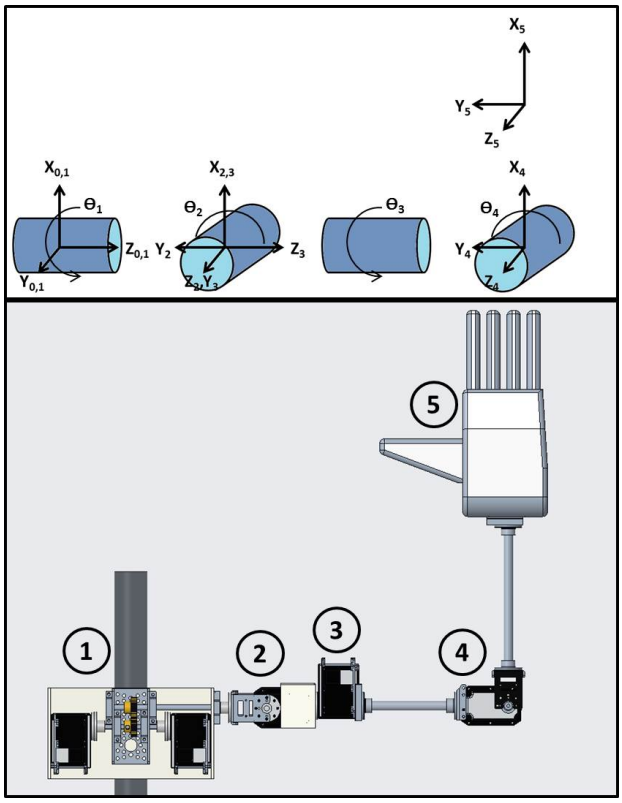

Fig. 3. A representation of our manipulator at its zero position with coordinate frames and revolute orientations for D-H Parameterization. The circled numbers in the lower image represent their corresponding frame in the upper image.

$$T_0^5 = T_0^1 T_1^2 T_2^3 T_3^4 T_4^5 \quad (2)$$

This represents the forward kinematic model of our manipulator.

B. Control methods

To facilitate one-to-one mapping of the remote user's gestures to joint positions, we consider two possible control methods. Both control methods used body tracking data from an Xbox Kinect to generate target trajectories for the arm to follow, extracting the user's elbow and hand position from the Kinect at a rate of 10 Hz and passing both through a 5-sample rolling average filter to dampen servo jitter produced by camera depth.

1) Direct arm mapping: The first control method uses the position of the user's shoulder, elbow, and hand to analytically determine the necessary joint targets. However this approach often produces discontinuous motion traversing the center of the body, such as a 180° rotation of Group 1 in Figure 1.

To produce more continuous motion we store the previous 5 joint targets. Each proposed solution is then compared to the average of the previous to determine which configuration would require minimum effort. The direct mapping motion produces a more accurate one-to-one mapping, but sacrifices smooth continuous motion to do so.

2) Inverse Kinematics: The memory of previous targets improves the arm behavior though still produces non-smooth movement. To combat noise we implement a full inverse kinematic model based on the FABRIK model proposed by Aristidou and Lasenby [27]. The FABRIK solution produces more continuous motion due to the fact that the constraints of the arm are leveraged to reduce the 6 axes (XYZ axes of the elbow and the hand) solution into a minimum effort solution of 3 axes (XYZ axes of the hand).

Using the Kinect alone we are unable to extract the orientation of the hand; only its position. As a result the kinematic solution is not fully constrained, allowing the model to drift away from a perfect mapping to the user in regards to elbow position. We are investigating ways to resolve the orientation of the hand allowing us to further constrain the solution without the need for peripheral attachments. The inverse kinematic solution sacrifices one-to-one mapping to produce smoother, more natural movement. Both methods of arm control will be evaluated in user studies to determine which is more important for productive communication.

C. Gimbal Lock

Joint angle variations exist largely in motion tracking when motion pathways are in close proximity to lines parallel to sensing pathways. This means Gimbal Lock is encountered frequently at $90°$ abduction from a free-hanging limb and any orientation where either the forearm or upper arm is adducted transversely towards the sensing pathway [28]. Inverse Kinematic solutions are sought out by restricting DOF solutions within regions near Gimbal Lock. For Forward Kinematics in this 4-DOF design, the Denavit-Hartenberg Convention is the most sensible method outside the areas where singularity is reached and is used in our Forward Kinematic simulations. For this problem, modeling the design using quaternion in conjunction with screw theory removes mathematical redundancies leading to Gimbal Lock and reduces computation time [29]. Future work will utilize this collaboration for both Forward and Inverse Kinematic solutions.

D. Workspace Visualization

The desired manipulator workspace is limited by (1) human limitations and (2) mechanical coupling limitations.

Transverse shoulder adduction is limited to $90°$ from neutral to prevent self-collision. Internal/External rotation is limited to $180°$ from neutral. Lateral abduction is limited to $180°$ above neutral. Elbow flexion is limited to $-90°$ and $20°$ due to hardware constraints. These can be seen in Figure 4. Though we have limited the workspace, we have done so minimally for minor collision prevention and to keep the usable workspace reasonably within the field of view of the remote user.

V. Fabrication and Prototype

The physical prototype is shown mounted on QB in Figure 5. The shoulder gearbox (Group 1 in Figure 1) is a 7.25" section of AL6061 U-channel secured to QB's neck via tapped grounding in a vertical configuration to prevent rotation about the neck axis. Housed within the channel are two Dynamixel MX-64T servos. The MX-64T has low-weight ($126g$), high-speed (26 rpm at peak torque), and high torque ($7.3Nm$ at stall). The first two servos are mounted inline on a $1/4$" D-shaft connected one-to-one to a 24T, $20°$ pressure-angle solid brass pinion. The pinion drives an identical gear connected to an output shaft.

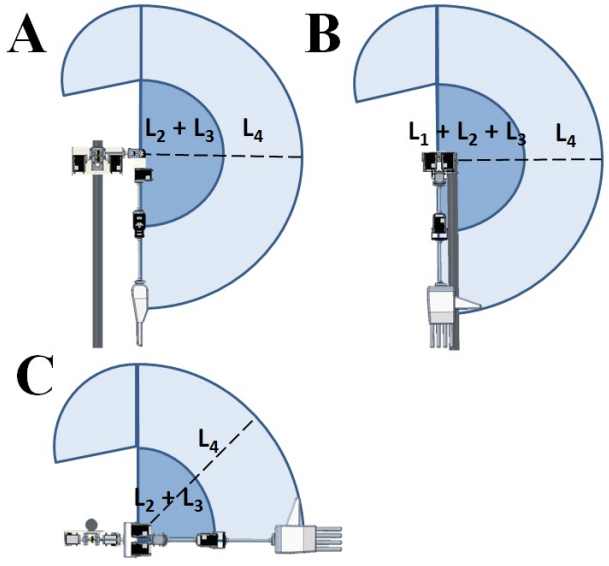

Fig. 4. **A**: Rear view, **B**: Side view, **C**: Top-down view of our manipulator overlaid with its planar operable workspace.

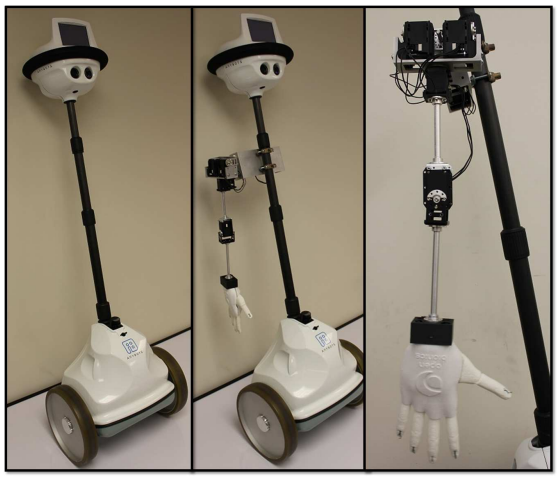

Fig. 5. (Left) QB without manipulator. (Middle) QB with manipulator. (Right) Side view of the manipulator.

The output shaft exits on a $1/4$" bearing housed in a pillow block mounted to the outside and connects with a Dynamixel synchronous-drive bracket. Two MX-64T servos are mounted in sync within a 4.50" AL6061 U-channel which rotates about the servo horn axis (Group 2 in Figure 1). A 5^{th} servo is mounted to the bottom of the U-channel as the shoulder's third DOF. This servo rotates a $10mm$ solid AL6061 rod upper arm. From the upper arm, a single Dynamixel bracket is mounted to a 6^{th} MX-64T servo serving as the fourth DOF.

The 6^{th} servo is directly linked to a $10mm$ solid AL6061 rod forearm. The total weight of the arm is $2.19kg$, well under the $20kg$ payload capcity of QB. A finite element analysis of Von Mises stress revealed a max stress on the gear teeth of $1.77ksi$; well below yield strength.

VI. Gesture Profile Validation

To illustrate and validate the manipulator's performance, we present 2 case studies actuating the manipulator on QB in profiles representative of 2 primary social behaviors. Specifically, we illustrate the manipulator performing a handshake motion (tangible interaction), a handwave motion (expressive gesture) [24].

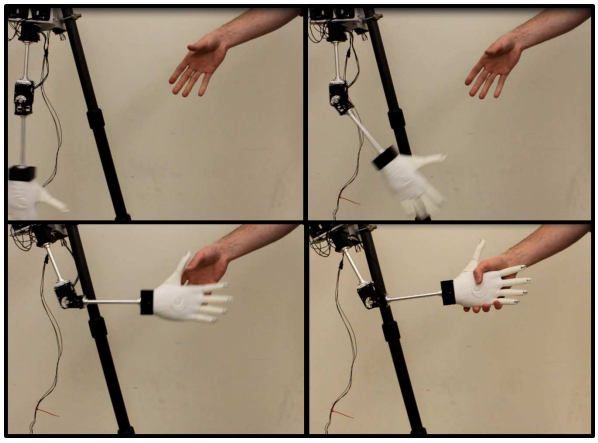

Fig. 6. The manipulator enacting the motion of shaking hands with a local user.

To generate these profiles, the manipulator was commanded to enact the entirety of the gesture by assigning a target angle to each joint. In addition, speed control was accomplished by assigning a time-from-start value to each position command that was determined by comparing the robot's movements to an average human gesture to achieve an appropriate anthropomorphic analogue. Position and angular velocity measurements were recorded during the actuation at a 50Hz frequency and logged to a file for data analysis. The results of these profiles and the corresponding change in their position are shown in Figure 7.

To calculate the velocity profile of our manipulator, we interpret the instantaneous position and velocity data into T_0^5 of our D-H transform series. A resulting vector series is created:

$$\mathbf{P} = \begin{bmatrix} P_x(\theta_{2,3,4,5}) \\ P_y(\theta_{2,3,4,5}) \\ P_z(\theta_{2,3,4,5}) \end{bmatrix} \tag{3}$$

The Jacobian of $\left[\ \mathbf{P}\ \right]$ is calculated as the time derivative of a function with respect to the derivative of the angular position:

$$\frac{\partial f}{\partial \theta} = \begin{bmatrix} \frac{\partial f_1}{\partial \theta_1} & \cdots & \frac{\partial f_1}{\partial \theta_n} \\ \vdots & \ddots & \vdots \\ \frac{\partial f_m}{\partial \theta_1} & \cdots & \frac{\partial f_m}{\partial \theta_n} \end{bmatrix} \tag{4}$$

The resulting velocity profile is a function of the angular velocities and Jacobian:

$$\dot{x} = \frac{\partial f}{\partial \theta}\left[\mathbf{P}\right]_\theta \overrightarrow{\theta} \tag{5}$$

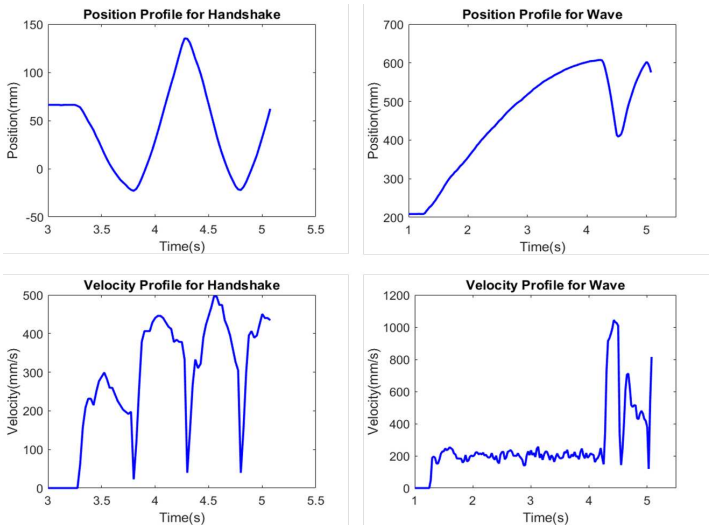

Fig. 7. Velocity magnitude profiles for a handshake and wave with respect to their position profile.

As shown in Figure 7, we observe that the handshake motion is periodic in nature, with an expected peak-to-peak amplitude [30]. The velocity profile also follows expected behavior, with sharp changes at the inflection points. The velocity values observed for the handshake fall within the range of the median velocity of $600\frac{mm}{s}$ for comparable human handshakes [30]. Similarly, the hand wave motion also exhibits an expected position profile, ramping the forearm up to the desired location, and then exhibiting oscillatory motion. The velocity profile associated with the hand wave falls within the range of the median velocity of $400\frac{mm}{s}$ for human hand waves [31]. We also note that our manipulator was operating at approximately 60% maximum speed in these case studies, illustrating that there is room for higher speed interactions if desired. For brevity, the pointing motion (the third primary social behavior) is omitted here, though we note that similar results were obtained in both the position and velocity, which is not surprising given the less dynamic requirements of pointing as compared to the other two primary behaviors evaluated here.

In addition to the expressive gesture validation case studies, we performed initial torque tests which demonstrated the capability of the selected servos to perform under maximum loads. An equivalent load of $2.92Nm$ at Group 1 was actuated dynamically through all orientations of the feasible workspace with no stalling or overheating in the motors. These tests were performed with direct motor control outside the realm of one-to-one mapping. Further testing showed no such problems with binding, stalling, or overheating when the prototype was actuated through all workspace variations. Taken together, these performance tests coupled

with our gesturing case studies illustrate the functionality of the designed manipulator and its support of enabling social interactions onboard telepresence platforms.

VII. Conclusion

In this work, we design and prototype a lightweight, robust, ergonomic manipulator with a heavy, anthropomorphic hand specifically for use on telepresence robots to enable enhanced social interactions. We present and validate its design and achievable workspace, coupled with initial design tests demonstrating its capabilities. Future work will include hands-free, active, one-to-one mapping of remote user movement using the Microsoft Kinect backbone, acceleration profile mapping to Laban Movement Analysis dictated emotional states, quaternion and screw theory implementation in both forward and inverse kinematic mapping, and a series of user studies exploring how expressive capabilities positively affect the social experience.

VIII. Acknowledgment

This work was funded by the National Science Foundation under Awards #1618926 and #1618283.

References

[1] K. Tanaka, H. Nakanishi, and H. Ishiguro, "Physical embodiment can produce robot operator's psuedo presence," *Frontiers in ICT*, vol. 2, no. 8, 2015.

[2] K. M. Tsui, M. Desai, H. A. Yanco, and C. Uhlik, "Exploring use cases for telepresence robots," *ACM/IEEE International Conference on Human-Robot Interaction*, pp. 11–18, 2011.

[3] F. Tanaka, "Robotics for supporting childhood education," *Cybernics: Fusion of human, machine and information systems*, pp. 185–195, 2014, chapter 10 Robotics for Supporting Childhood Education.

[4] F. Tanaka, T. Takahashi, S. Matsuzoe, N. Tazawa, and M. Morita, "Telepresence robot helps children in communicating with teachers who speak a different language," *ACM/IEEE International Conference on Human-Robot Interaction*, pp. 399–406, 2014.

[5] M. Anvari, "Robot-assisted remote telepresece surgery," *Surgical Innovation*, no. 11, pp. 123–128, June 2004.

[6] J. Gonzalez-Jimenez, C. Galindo, and J. R. Ruiz-Sarmiento, "Technical improvements of the giraff telepresence robot based on users' evaluation," *IEEE RO-MAN Conference*, pp. 827–832, 2012.

[7] E. Dreyfuss, "My life as a robot," *WIRED*, Sept. 2015, http://www.wired.com/2015/09/my-life-as-a-robot-double-robotics-telecommuting-longread/.

[8] D. Sakamoto, T. Kanda, T. Ono, H. Ishiguro, and N. Hagita, "Android as a telecommunication medium with a human-like presence," *2nd ACM/IEEE International Conference on Human-Robot Interaction*, pp. 193–200, 2007.

[9] V. A. Newhart, "Virtual inclusion via telepresence robots in the classroom," *Extended Abstracts on Human Factors in Computing Systems*, pp. 951–956, 2014.

[10] F. Tanaka, A. Cicourel, and J. R. Movellan, "Socialization between toddlers and robots at an early childhood education center," *Proceedings of the National Academy of Sciences*, vol. 104, no. 46, pp. 17 954–17 958, november 13th 2007.

[11] H. Nakanishi, K. Tanaka, and Y. Wada, "Remote handshaking: touch enhances video-mediated social telepresence," *Proceedings of the 32nd annual ACM conference on Human factors in computing systems*, pp. 2143–2152, 2014.

[12] T. Asfour, K. Regenstein, P. Azad, J. Schroder, A. Bierbaum, N. Vahrenkamp, and R. Dillmann, "Armar-iii: An integrated humanoid platform for sensory-motor control," *6th IEEE-RAS International Conference on Humanoid Robots*, pp. 169–75, 2006.

[13] M. Hirose and K. Ogawa, "Honda humanoid robots development," *Philosophical Transactions of the Royal Society A: Mathematical, Physical and Engineering Sciences*, vol. 365, no. 1850, pp. 11–19, 2007.

[14] C. S. Lovchik and M. A. Diftler, "The robonaut hand: A dexterous robot hand for space," *IEEE International Conference on Robotics and Automation*, vol. 2, pp. 907–912, 1999.

[15] G. Metta, G. Sandini, D. Vernon, L. Natale, and F. Nori, "The icub humanoid robot: an open platform for research in embodied cognition," *Proceedings of the 8th Workshop on Performance Metrics for Intelligent Systems*, pp. 50–56, 2008.

[16] N. Fukaya, S. Toyama, T. Asfour, and R. Dillmann, "Design of the tuat/karlsruhe humanoid hand," *IEEE/RSJ International Conference on Intelligent Robots and Systems*, vol. 3, pp. 1754–1759, 2000.

[17] S. Roccella, M. C. Carrozza, G. Cappiello, P. Dario, J. J. Cabibihan, M. Zecca, H. Miwa, K. Itoh, and M. Marsumoto, "Design, fabrication and preliminary results of a novel anthropomorphic hand for humanoid robotics: Rch-1," *IEEE/RSJ International Conference on Intelligent Robots and Systems*, vol. 1, pp. 266–271, 2004.

[18] K. Kaneko, K. Harada, F. Kanehiro, G. Miyamori, and K. Akachi, "Humanoid robot hrp-3," *IEEE/RSJ International Conference on Intelligent Robots and Systems*, pp. 2471–2478, 2008.

[19] G. Hirzinger, J. Butterfass, M. Fischer, M. Grebenstein, M. Hahnle, H. Liu, I. Schaefer, and N. Sporer, "A mechatronics approach to the design of light-weight arms and multifingered hands," *IEEE International Conference on Robotics and Automation*, vol. 1, pp. 46–54, 2000.

[20] K. Kaneko, K. Harada, and F. Kanehiro, "Development of multifingered hand for life-size humanoid robots," *IEEE International Conference on Robotics and Automation*, pp. 913–920, 2007.

[21] S. Schulz, C. Pylatiuk, A. Kargov, R. Oberle, and G. Bretthauer, "Progress in the development of anthropomorphic fluidic hands for a humanoid robot," *IEEE/RAS International Conference on Humanoid Robots*, pp. 566–575, 2004.

[22] Y. K. Lee and I. Shimoyama, "A skeletal framework artificial hand actuated by pneumatic artificial muscles," *IEEE International Conference on Robotics and Automation*, pp. 926–931, 1999.

[23] G. Yang, W. Lin, M. S. Kurbanhusen, C. B. Pham, and S. H. Yeo, "Kinematic design of a 7-dof cable-driven humanoid arm: a solution-in-nature approach," *Proceedings of the 2006 IEEE/ASME International Conference on Advanced Intelligent Mechatronics*, 2006.

[24] R. Mead, A. Atrash, E. Kaszubski, A. St. Clair, J. Greczek, C. Clabaugh, B. Kohan, and M. J. Mataric, "Building blocks of social intelligence: Enabling autonomy for socially intelligent and assistive robots," *AAAI Fall Symposium on Artificial Intelligence and Human-Robot Interaction*, November 2014.

[25] R. Contini, "Body segment parameters, part ii," *Artificial Limbs, Vol. 16, No. 1, pp. 1-19*, 1972.

[26] K. DeGoede, "How quickly can healthy adults move their hands to intercept an approaching object? age and gender effects," *The Journals of Gerontology*, pp. M584–M588, 2001.

[27] A. Aristidou and J. Lasenby, "FABRIK: A fast, iterative solver for the inverse kinematics problem," *Graphical Models*, vol. 73, no. 5, pp. 243–260, 2011.

[28] P. Salvini, C. Laschi, and P. Dario, "Adapting human motion for the control of a humanoid robot," *International Conference on Robotics and Automation*, pp. 1390–1397, 2002.

[29] E. Sariyildiz and H. Temeltas, "Solution of inverse kinematic problem for serial robot using quaterninons," *International Conference on Mechatronics and Automation*, pp. 26–31, 2009.

[30] M. Jindai and T. Watanabe, "Development of a handshake robot system based on a handshake approaching motion model," *IEEE/ASME international conference on advanced intelligent mechatronics*, 2007.

[31] J. H. Seo, J. Y. Yang, and D. S. Kwon, "Generation of various hand-waving motion of a humanoid robot in a greeting situation," in *11th International Conference on Ubiquitous Robots and Ambient Intelligence (URAI)*, 2014.